



Original Paper

Construction of complex digital rock physics based on full convolution network



Jia Kang^a, Nian-Yin Li^{a,*}, Li-Qiang Zhao^a, Gang Xiong^b, Dao-Cheng Wang^b, Ying Xiong^b, Zhi-Feng Luo^a

^a State Key Laboratory of Oil and Gas Reservoir Geology and Exploitation Engineering, Southwest Petroleum University, Chengdu, 610500, Sichuan, China

^b Research Institute of Natural Gas Technology, Southwest Oil and Gas Field Company, PetroChina, Chengdu, 610213, Sichuan, China

ARTICLE INFO

Article history:

Received 31 August 2021

Accepted 15 November 2021

Available online 20 November 2021

Edited by Yan-Hua Sun

Keywords:

Digital rock physics

Depth learning

U-Net

Complex core

Complex fracture

ABSTRACT

Digital rock physics (DRP) is a paramount technology to improve the economic benefits of oil and gas fields, devise more scientific oil and gas field development plans, and create digital oil and gas fields. Currently, a significant gap is present between DRP theory and practical applications. Conventional digital-core construction focuses only on simple cores, and the recognition and segmentation effect of fractures and pores of complex cores is poor. The identification of rock minerals is inaccurate, which leads to the difference between the digital and actual cores. To promote the application of DRP in developing oil and gas fields, based on the high-precision X-ray computed tomography scanning technology, the U-Net deep learning model of the full convolution neural network is used to segment the pores, fractures, and matrix from the complex rock core with natural fractures innovatively. Simultaneously, the distribution of rock minerals is divided, and the distribution of rock conditions is corrected by X-ray diffraction. A pore–fracture network model is established based on the equivalent radius, which lays the foundation for fluid seepage simulation. Finally, the accuracy of the established a digital core is verified by the porosity measured via nuclear magnetic resonance technology, which is of great significance to the development and application of DRP in oil and gas fields.

© 2021 The Authors. Publishing services by Elsevier B.V. on behalf of KeAi Communications Co. Ltd. This is an open access article under the CC BY-NC-ND license (<http://creativecommons.org/licenses/by-nc-nd/4.0/>).

1. Introduction

Efficient development of oil and gas fields is inseparable from scientific and reasonable development plan design. The development plan is mainly based on the experimental evaluation results of oil and gas reservoir rocks, such as rock porosity, permeability, water saturation, mineral type and contents (Shirangi and Durlofsky, 2015). The acquisition of reservoir rock is a very difficult process, which is often buried thousands of meters below. Generally, it is obtained in the process of drilling. This often leads to two major problems. First, the drilling process is very destructive, and some rocks with strong brittleness and weak mineral bond strength will be broken. Second, the same well can only drill rocks once at any depth, and the number of rocks drilled is small, and the number of rocks with the same lithology is less. The destruction of rock and the small amount of rock will seriously restrict the effect

of laboratory evaluation experiment. When comparing the damage of different fracturing fluids to rocks, inaccurate experimental results are often obtained because of the different physical properties of rocks. When evaluating the acidizing effect of different acid, the difference in rock mineral compositions will significantly influence the acidizing effect. On the other hand, there are various types of laboratory evaluation experiments for rocks, and the number of experiments is huge. To obtain excellent evaluation results, the number of rocks is often inadequate. For some unconventional low permeability reservoir rocks, the experimental evaluation is more difficult. Sometimes a set of fracturing fluid damage tests can take an entire day, and a set of long-term conductivity tests can take several months, which is extremely inefficient. Based on these problems, the conventional physical evaluation technology is unable to develop the oil and gas field to meet higher efficiency. With the rapid development of digital science and technology, digital rock physics (DRP) technology has been widely discussed by researchers in the field of oil and gas field development (Al-Marzouqi and Hasan, 2018), and is also the key direction for oil and gas field

* Corresponding author.

E-mail address: lnyswpu@163.com (N.-Y. Li).

development workers. DRP can have the following properties. (1) Fast calculation speed and low cost: once the three-dimensional (3D) digital core is established, it can be reused, and the data of conventional and special petrophysical experiments can be obtained much faster than in the laboratory. (2) Flexible selection of test samples: conventional laboratory analysis requires high-quality plunger rock samples, and digital core technology can perform 3D digital core construction and numerical simulation analysis on almost all rock samples, such as cuttings, loose sandstone, old core, damaged core, and sidewall coring; DRP experiments can be used to replace conventional petrophysical experiments to a certain extent. (3) Strong controllability: DRP can adjust the microparameters of the 3D digital core as desired, and DRP experiments are helpful to understand the influence of rock microparameters on reservoir macro physical properties. (4) Green environmental protection: DRP does not need to use chemical reagents harmful to the environment. At present, there is a big difference between the theoretical research and practical applications of DRP. The main problem is that the internal structure of rocks is complex, the shape of rock particles is diverse, and the identification accuracy of rock fractures and matrix is low. Therefore, it is difficult to build the same seepage channel as the real rock, and the actual evaluation effect cannot be obtained, which seriously restricts the large-scale application of DRP. Once it can be applied on a large scale and efficiently, it will provide significant help to global oil and gas production. This study focuses on the high-precision identification of rock fractures and lays the foundation for constructing high-precision DRP.

Fracture recognition of DRP belongs to the image segmentation category. From the 1960s until deep learning (DL) became widely used in the imaging field, researchers have proposed thousands of methods for image segmentation, such as threshold-, edge-, region-, graph theory-, clustering-, and fuzzy theory-based methods (Forkert et al., 2013; Saad et al., 2011; Stadlbauer et al., 2004; Zhao et al., 2014) as well as other methods combined with specific theories and tools. However, most of these methods use the medium- and low-order visual information of image pixels, such as color, texture, shape, roughness, directivity, and compactness correlations. These methods have good segmentation ability for specific background, but the performance in more complex tasks is unsatisfactory. Therefore, no universally applicable segmentation technology has been proposed at present, and it is often necessary to combine the prior knowledge of relevant fields to carry out effective segmentation.

Knackstedt et al. (2009) used 3D X-ray microscopic imaging technology to analyze the pore structure and physical properties of carbonate rocks; this technology is an advanced and scientific core analysis technology different from conventional methods for analyzing the pore and grain structure of rock materials (e.g., mercury injection, sieving, and petrochemical thin section). The carbonate rocks in this paper have no fractures, and it is not difficult to see that the simplest threshold segmentation method is used in matrix segmentation. Claudio et al. (2012) discussed the relationship between rock elastic characteristics and rock mineral composition when studying rock elastic characteristics. In this study, the recognition of minerals is based on the naked eye and personal experience. Saenger et al. (2011) discussed the influence of rock elasticity and fluid viscosity. After using the threshold segmentation method to identify pores and matrix, some invalid independent pores were manually removed. The study could reduce the complexity of DRP, but the processing time was very long and efficiency was low. Andra et al. (2013) used a Fontainebleau sandstone sample (porosity 0.147), a grayscale Berea sample and a grayscale Grosmont carbonate sample to segment the pores and matrix independently. Based on the threshold segmentation

method, the gray value of each part is used for threshold segmentation after computed tomography (CT) scanning, which has great uncertainty and is difficult to segment pores and microfractures effectively. Saxena et al. (2018) proposed the construction of digital petrophysics with low-resolution CT scanning technology and the seepage simulation. It was found that at least 10 voxels were needed to fully simulate the seepage of single-phase flow in the pore throat, and low-resolution CT scanning technology would be gradually abandoned in future research. In addition, they used the best threshold segmentation method in the recognition of matrix and pores, which is not the best choice. We will discuss this problem later. Kelly et al. (2016) used the threshold segmentation method based on cluster analysis to divide the gray value of FIB-SEM scanning in the target rock slice into six categories as well as obtained pore, matrix, and other attributes, respectively, which improved the accuracy of threshold classification to a certain extent, but in essence, the segmentation effect was still unideal, and the segmentation effect of pores and microfractures was poor, most of the time, microfractures are wrongly classified as pores. Al-Marzouqi and Hasan (2018) reported that the threshold segmentation algorithm of global pixels was unconvincing to the segmentation of some regions with uneven gray distribution, and 3D hierarchical segmentation algorithms that analyze the spatial distribution of gray were better methods for image segmentation.

In summary, pore and fracture segmentation of DRP is based on the conventional threshold segmentation method, and the segmentation effect is poor. However, in the field of medicine, artificial intelligence, and so on, DL technology has been used to achieve image semantic segmentation, such as the recognition of brain tumors and osteoporosis, which are high-precision tasks. In 2014, the first full convolution network (FCN) for image segmentation was proposed (Long et al., 2015). In 2015, the U-Net FCN image segmentation technology championed the International Symposium on Biomedical Imaging (ISBI) cell tracking challenge. The fast and high efficiency of image segmentation of this technology has attracted significant research attention (Ronneberger et al., 2015). This technology inspired the construction of digital-physical rock pore and fracture structures, which can realize high-precision identification of fractures and pores and separate them from the matrix. In addition, through DL, the technology can distinguish microcracks and cracks that are fuzzy to the naked eye from pores, which solves the difficulty of manual segmentation. This technology improves the theoretical basis for efficient and high-precision construction of digital-physical rock; in this study, we investigate the fracture identification technology based on DL.

2. X-ray

X-ray CT scanning and digital core analysis are increasingly used to calculate porosity and permeability from millimeter to centimeter scales in geosciences. The first step of establishing DRP is to obtain the internal structure of the core using X-ray CT scanning technology (Karimpouli et al., 2019). DRP can characterize the microstructure of rocks on the pore scale and quantitatively study the relationship between rock physical parameters and properties. Dvorkin et al. (2009) and Kuntz et al. (2000) employed DRP to study physical properties of cores, including acoustic properties, electrical properties, nuclear magnetic resonance (NMR) relaxation, and permeability. With the improvement of the accuracy of CT scanning technology and the acceleration of industrialization, DRP has developed rapidly, making it possible to clearly capture and visualize the 3D pore geometry of reservoir rock (Kalam et al., 2013; Riepe et al., 2011). The higher the accuracy of CT scanning the smaller is the resolution, and the more accurate is the rock microstructure displayed via filtered back projection (FBP) (Arns

et al., 2002). Through a series of image processing methods such as filtering to eliminate noise signal and image segmentation, we can perform digital processing of rocks, realize a digitization of pore structures, fracture structures, and matrix, as well as integrate fluid flow characteristics and other rock characteristics, such as elastic modulus, formation resistivity, and relative permeability (Saenger et al., 2004; Schembre et al., 2003; Taud et al., 2005). Andra et al. (2013) discussed the segmentation of gray value of CT scanning results in detail, and compared the segmentation effect of four types of rock samples. In addition, the uncertainty of image segmentation was discussed, which showed the weakness and low efficiency of conventional segmentation methods in the face of a strong heterogeneous core. For establishing digital cores, image segmentation, that is, the segmentation of holes, fractures, and matrix, is crucial. At present, DL technology, as a global research hotspot, can intelligently analyze the internal laws of data, and is an important tool to solve the problem of core CT scan image segmentation. This technology is the general trend.

In this study, a micro XCT-400 instrument was used to scan cores. The rock samples were obtained from the oil reservoir. They were dense, heterogeneous, and had complex natural fractures (Fig. 1).

As the main target of this study is natural fractures, which are large in scale, the scanning resolution is 10 μm , and the scanning results of some rock samples were intercepted for subsequent processing. After CT scanning, the common FBP method was used to perform the digital reconstruction of 3D cores and the reconstruction results are shown in Fig. 2.

From the scanning results, the core contained large natural fractures and some secondary fractures. Overall, the fracture morphology is more complex, which is a good research target for fracture identification and extraction technology. The DRP reconstructed by the FBP method will inevitably produce noise signal, which hinders the accurate identification of fractures. Therefore, it is necessary to eliminate the noise, which is a crucial part of digital core preprocessing.

3. Noise elimination

There are three main sources of noise in CT scanning. (1) Quantum noise: this is a kind of readout noise in the experimental observation, which is distributed by Poisson. When the number of

X-ray photons in the observation is less than that of the number of observable statistical fluctuations in the data readout on the detector, the statistical fluctuation of this kind of readout is called quantum noise. It is the main noise in low-dose CT. (2) The noise introduced by the inherent limitation of a CT hardware system: this mainly includes the electronic noise in photodiodes, the noise of the point noise introduced in the data acquisition system, and the noise of X-ray scattering. Such noise cannot be avoided and is unaffected by human control and can be reduced by improving the hardware system, but it cannot be eliminated. (3) The noise introduced in the reconstruction of CT images: in this study, the first two noises will not be considered; instead, this third noise signal will be reduced to optimize the quality of digital cores while keeping the details of cores as much as possible. There are many methods to eliminate noise at present, such as bilateral, box, Gaussian, medium, nonlocal means, and anisotropic diffusion filters. The digital core noise elimination will be shown with a section of the core, as shown in Fig. 3.

The six filtering effects are good mainly due to the low complexity of the gray image, low color contrast of each part, and smooth gray change. Therefore, filtering algorithms with good detail retention have good advantages in DRP. In fact, the physical properties of rocks —fractures and pore sizes— and the distribution of mineral composition are all spatially related, whether in cores or strata. Sometimes, the parts that are not directly connected will show the same attributes. The filter can show a strong advantage, it considers the correlation between core gray and geometric structure similarity, has a strong advantage and potential for digital core noise elimination. Finally, the nonlocal means filter method is adopted in this study. The conventional identification technology determines an optimal threshold segmentation point, and then the matrix and pore are segmented. At this time, the fracture is determined as a pore. Alternatively, two threshold segmentation points are determined to segment matrix, pore, and fracture.

4. Conventional segmentation technology

Conventional image semantic segmentation mainly includes threshold segmentation, clustering analysis, and boundary detection methods. At present, research on fracture identification is very few, and most of the research still uses threshold segmentation for

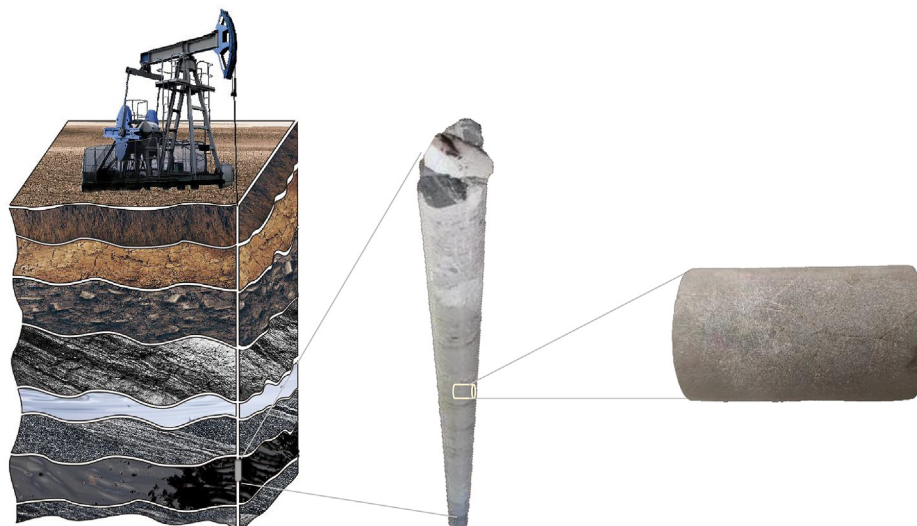


Fig. 1. Core acquisition process.

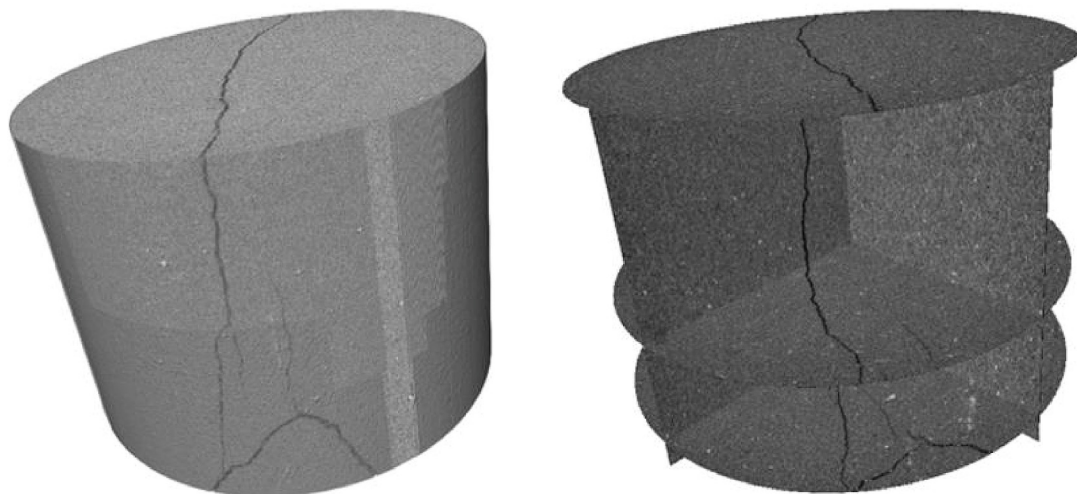
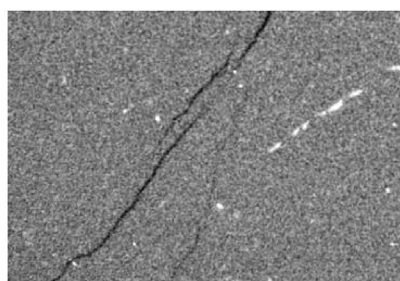
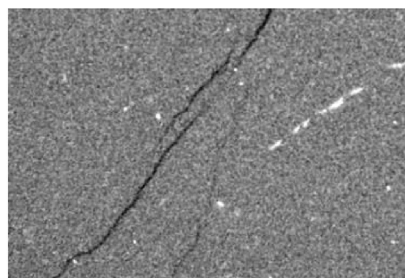


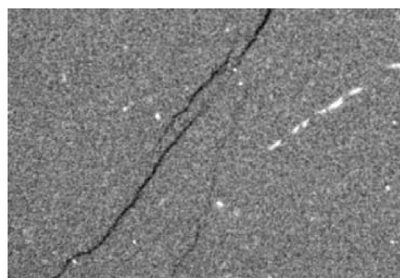
Fig. 2. Results of digital core reconstruction by FBP after CT scanning.



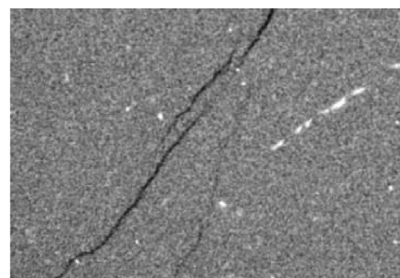
(a) Original rock sample



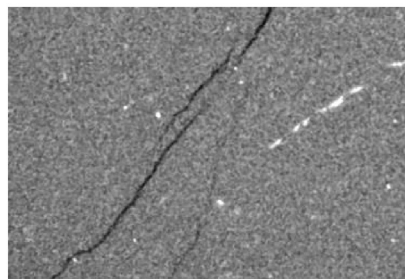
(b) Bilateral filter



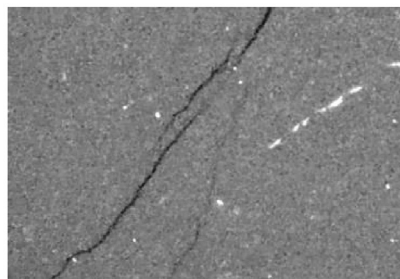
(c) Box filter



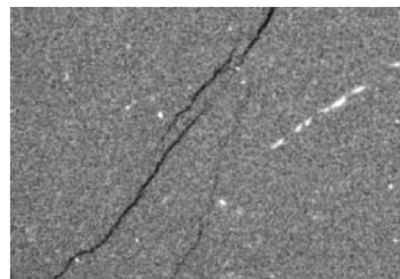
(d) Gaussian filter



(e) Median filter



(f) Nonlocal means filter



(g) Anisotropic diffusion filters

Fig. 3. Noise elimination of digital core.

pore identification. The conventional identification method focuses on determining 1–2 optimal threshold segmentation points to segment matrix, pore, and fracture. The maximum interclass variance method is an excellent method in threshold segmentation, which has the advantages of a simple algorithm, stable

performance, and low calculation complexity. Next, the disadvantages of conventional threshold segmentation technology are described on the basis of its algorithm. The interclass variance of an image is as follows:

$$g(t) = \omega_1(\overline{gray}_1 - gray)^2 + \omega_2(\overline{gray}_2 - gray)^2 \tag{1}$$

with

$$gray = \omega_1 \times \overline{gray}_1 + \omega_2 \times \overline{gray}_2 \tag{2}$$

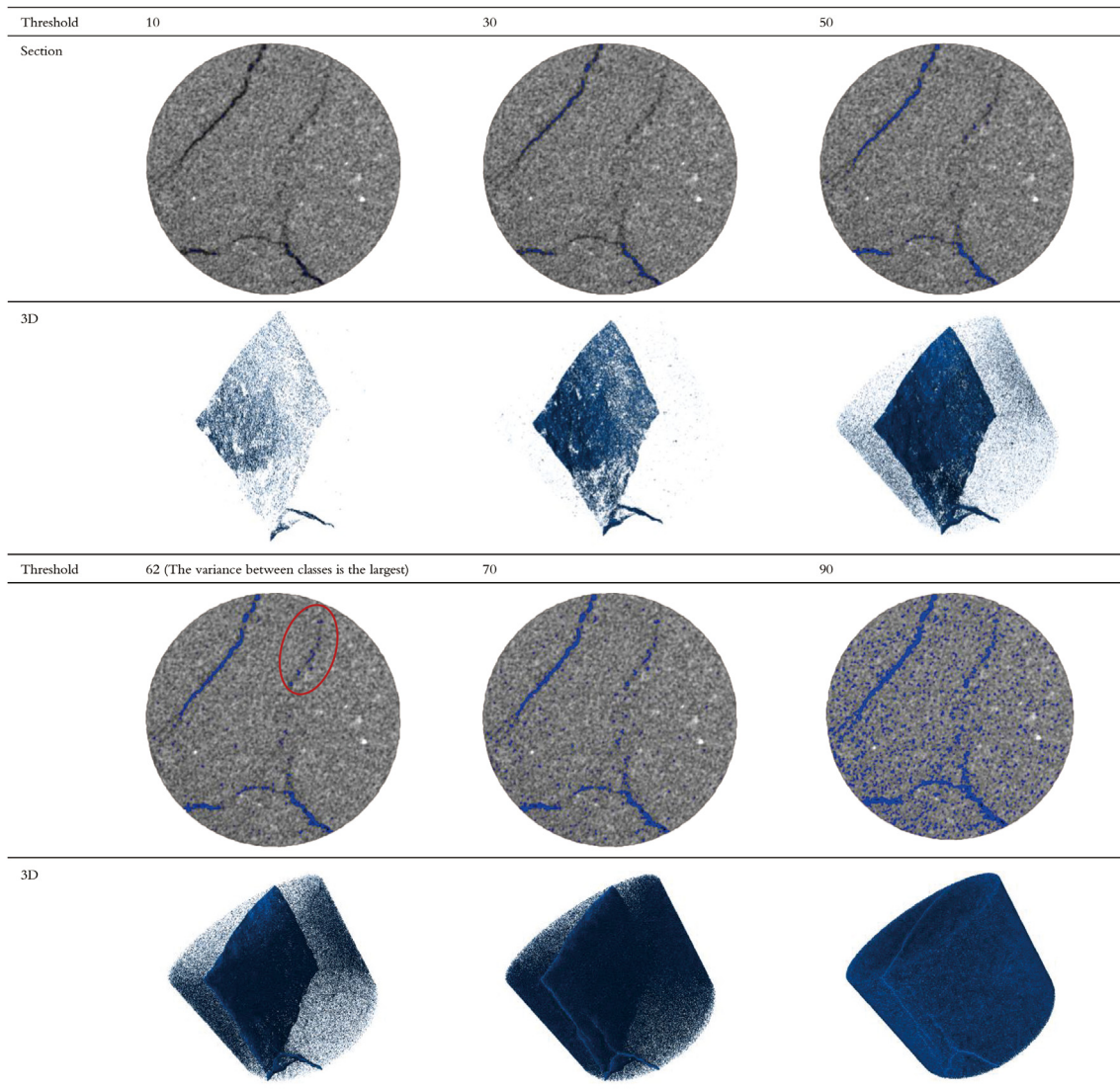
where ω_1 is the proportion of the number of background group pixels in the entire image; ω_2 is the proportion of the number of pixels in the target group in the entire image; \overline{gray}_1 is the background group average gray; \overline{gray}_2 is the average gray level of the target group.

When the variance between classes is the largest, the corresponding gray value is the best segmentation threshold. This method is widely used and is the most classic method of global binarization. The segmentation effect of conventional threshold segmentation method is shown in Table 1.

It is not difficult to see that the conventional threshold segmentation method is unsuitable for core segmentation with strong

heterogeneity. When the gray threshold is set to 70, the fracture can be best segmented, but a large number of pores and even part of the matrix will be wrongly determined as fractures, belonging to serious over-segmentation, which is atrocious for the subsequent establishment of a pore model. The wrong flow path will be established. Even when the interclass variance is maximum, most fractures can be identified, but a large number of pores are mistakenly identified as fractures. This is the biggest drawback of the conventional pore recognition technology for fracture recognition; it is difficult to accurately segment fractures. In addition, in the place of low gray contrast, the continuous fractures with spatial correlation will be recognized as a large number of independent pores. For instance, when the variance between classes is the largest, that is, when the gray threshold is 62 (the part coiled up by the red box) continuous fractures are identified as a large number of independent pores. This is also a factor that seriously restricts the application and development of digital core in the oilfield. Next, we focus on solving this problem using DL.

Table 1
Segmentation effect of conventional threshold segmentation method.



5. DL technique

The semantic segmentation method of image based on DL is divided into two parts: region-based semantic segmentation and pixel classification-based image semantic segmentation methods. The DL technology is based on U-Net FCN image segmentation technology. The reasons for this technology are as follows. (1) Core image semantics is simple, fracture and pore structures are relatively fixed, skip connection and the U-shaped structure of the U-Net model are excellent for advanced semantic information and low-level feature processing. (2) The U-Net model is suitable for the reservoir with too much data, such as the ultradeep unconventional reservoir or reservoir whose core is difficult to be drilled completely. (3) The U-Net model has a good segmentation of core matrix, pore, and fracture; therefore, it can be used to establish core matrix, pore and fracture network model for accurate simulation of flow, which has important significance.

The U-Net model is in full convolution form, without a full connection layer (that is, there is no fixed graph size), so it is easy to adapt to many input sizes, but not all sizes can be determined according to the network structure. In U-Net, pooling is 2×2 and is a valid policy, that is, there is no padding. Therefore, it is necessary to ensure that the input image has an even side length when it passes through the pooling every time. So, special attention should be paid to the size of the input image. A better method is to start from the minimum resolution (the resolution is the size of the feature map) and calculate toward the shrinkage path to realize the size of the input image (see Fig. 4).

U-Net uses the loss function with boundary weight:

$$E = \sum_{X \in \Omega} \omega(X) \log(p_{l(X)}(X)) \tag{3}$$

with

$$\omega(X) = \omega_c(X) + \omega_0 \cdot \exp\left(-\frac{(d_1(X) + d_2(X))^2}{2\sigma^2}\right) \tag{4}$$

$$p_k(X) = \frac{\exp(a_k(X))}{\sum_{k=1}^K \exp(a_k(X))} \tag{5}$$

where l is the label value of the pixel; ω is the weight of the pixel; d_1 is the distance from a pixel point to the nearest fracture or pore; d_2 is the distance from a pixel point to the second nearest fracture or pore; ω_c is the weight map to balance the class frequencies; ω_0 and σ are constants.

To make the follow-up research results more convenient for readers to observe, we will further narrow the research area and focus on the area with relatively developed fractures (Fig. 5) and use 50 learning data for training. The training data mainly comes from the author's research team's manual segmentation of a large number of core fractures and pores in the process of digital core research in recent 5 years. One of the learning data is as follows. The training data are manually selected, and the big data can be edited through Boolean operation in the selection process.

After 42 training times, and the training effect was good, and the change in the loss value with the number of training is shown in Fig. 6.

After 25 training times, the loss value was stable at approximately 0.05, and the final training stops after the 42nd training. The recognition effect of fractures and pores was excellent (Fig. 7).

The U-Net model could segment fractures and pores efficiently. There was a large number of small strip fractures in the middle of Fig. 7(a), which might be the microfractures produced after stress unloading during core removal from the reservoir to ground.

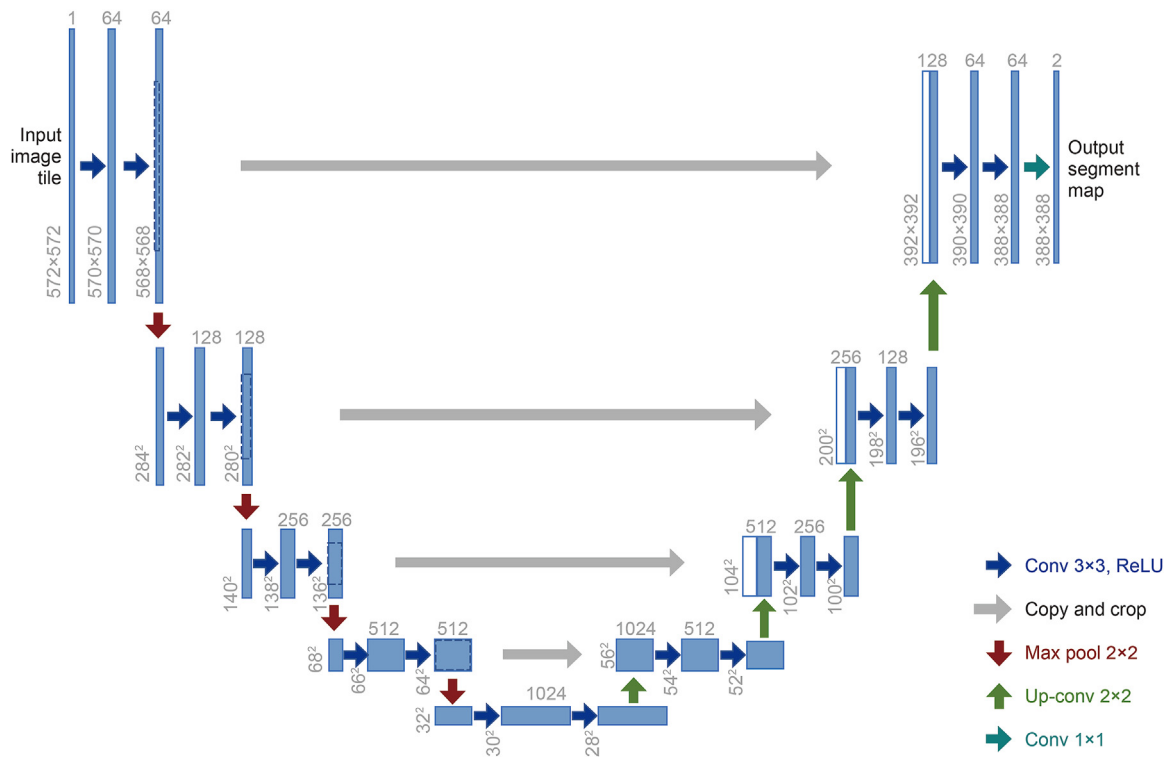


Fig. 4. U-Net architecture (example for 32×32 pixels in the lowest resolution). Each blue box corresponds to a multichannel feature map. The number of channels is denoted on top of the box. The x - y -size is provided at the lower-left edge of the box. White boxes represent copied feature maps. The arrows denote the different operations (Ronneberger et al., 2015).

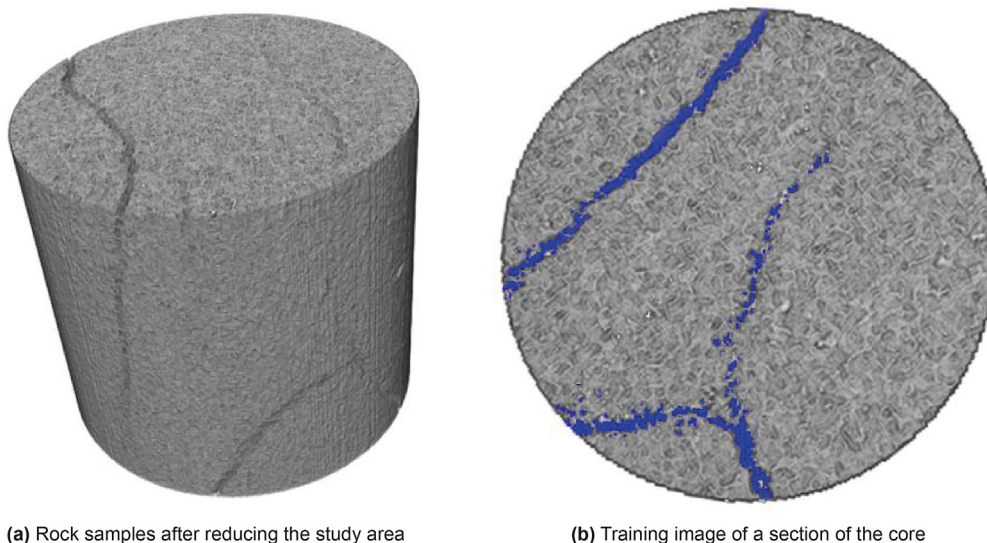


Fig. 5. Research and training objectives after reduction.

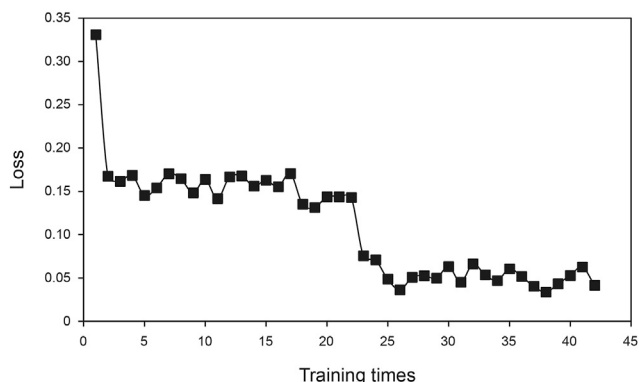


Fig. 6. The change of loss value in the process of data training.

Generally, this was difficult to identify, indicating that the model had a good image semantic segmentation effect. In addition, some pores at the edge of the fracture were determined as fractures, which were inevitable, because they had a strong spatial correlation with fractures, and the resulting error was rational.

By adding separated fractures and pores into the core (Fig. 8), it could be found that the U-Net model could well extract the pore characteristics of the cores and did not identify any internal space of fractures as a pore, that is, it retained the spatial correlation of pores and fractures. This is crucial for constructing pore–fracture network model of subsequent cores.

6. Construction of pore–fracture network model

The pore–fracture network model is based on capillary and equivalent radius theories, that is, the irregular pore space is

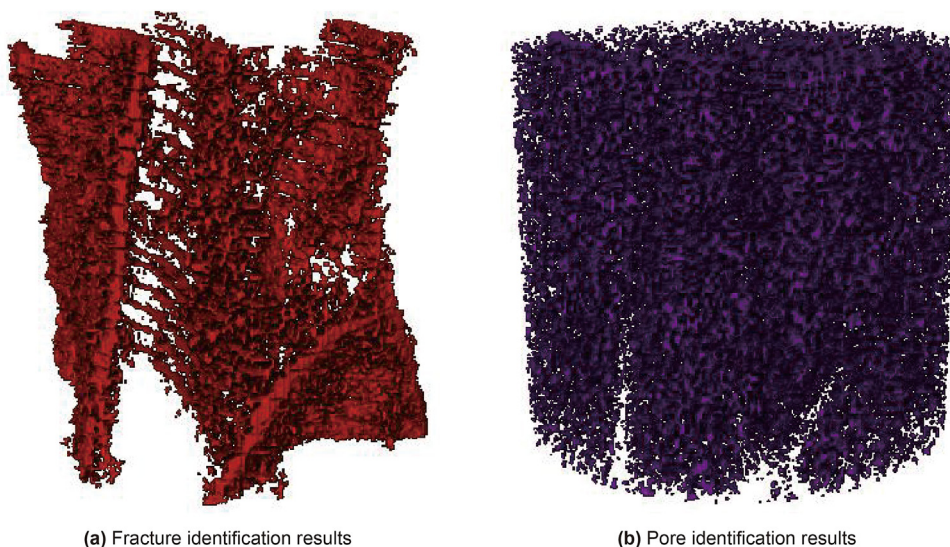


Fig. 7. Fracture and pore identification results based on U-Net.

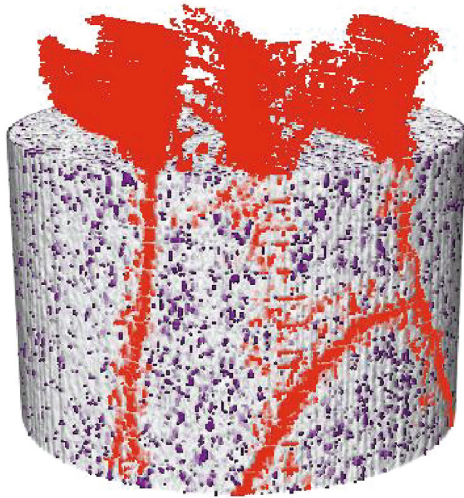


Fig. 8. Performance of fractures and pores in the rock core.

regarded as a sphere with the same volume, and roar channel is regarded as a cylindrical pipe with the same volume. The division of porosity and roar is based on the number of pores, n , in the 26 neighborhoods of any point. When the number of pores is less than 10, it will be judged as a roaring channel, and the rest will be identified as pores.

When $n \geq 10$, the target is determined to be a pore, which is represented by a sphere with an equivalent radius. The equivalent radius of the sphere is calculated as follows:

$$\sum_{i=1}^{26} \left(\sum_{k=0}^n V_{\text{voxel},k} \right)_i = \frac{4}{3} \pi r^3 \tag{6}$$

When $n < 10$, the target is judged as a roar, which is represented by a sphere cylindrical pipe with an equivalent radius. The equivalent radius of the cylinder pipe is calculated as follows:

$$\sum_{i=1}^{26} \left(\sum_{k=0}^m V_{\text{voxel},k} \right)_i = \pi R^2 L \tag{7}$$

$$L = m \times L_{\text{voxel}} \tag{8}$$

where n is the number of pores continuously determined from any direction of the 26 neighborhoods of a point; m denotes the number of consecutive roars determined from any direction of the 26 neighborhoods of a point; V_{voxel} represents the volume of a voxel in a digital core, μm^3 ; r is the equivalent radius of the pore, μm ; R is the equivalent radius of the roar, μm ; L_{voxel} is the length of a voxel, μm .

Through the deep learning process, the pores, fractures and matrix have been effectively segmented, and the pore and fracture data are substituted into the above formula for calculation to obtain the equivalent pore radius and roar radius. Thus, the network structure of pore–fracture is established (Figs. 9 and 10).

The equivalent radius of the core pore and roar channel was small, which indicated that the core pore roar was small and very dense. In addition, the fracture had good connectivity and could have a good seepage effect. If we wanted to use a digital core to efficiently simulate physical experiments, only the seepage is not enough. Most fluid displacement experiments involve an acid rock reaction, chemical adsorption, physical expansion, and other experimental processes. It is closely related to the mineral composition type, content, and distribution of the core, so the rock state attribute will be modeled next.

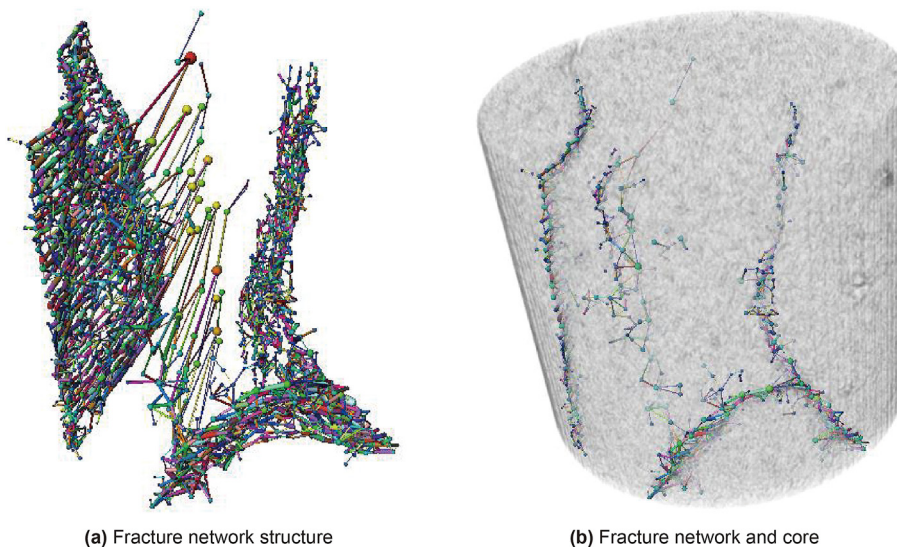
7. Rock mineral properties

The rock mineral composition mainly includes calcite, quartz, dolomite, orthoclase, plagioclase, and metal minerals, which mainly determines the chemical reaction between digital core and fluid, such as acid rock reaction. In addition, it contains clay composition, mainly including illite, kaolinite, and montmorillonite, which mainly determines the sensitivity of digital core, such as water, velocity, salt, and alkali sensitivity.

The mineral composition of the core was analyzed by DX-2700 X-ray diffractometer; the result is shown in Fig. 11.

The results showed that calcite accounts for 76.3% (CaCO_3), quartz 14.6% (SiO_2), and clay 9.1%. Researchers can subdivide clay minerals and model them more precisely.

According to the CT scanning pictures, the rock surface is scanned at fixed points by Quanta 450 environmental scanning electron microscope, and the energy dispersive X-ray spectroscopy



(a) Fracture network structure

(b) Fracture network and core

Fig. 9. Network structure of fractures.

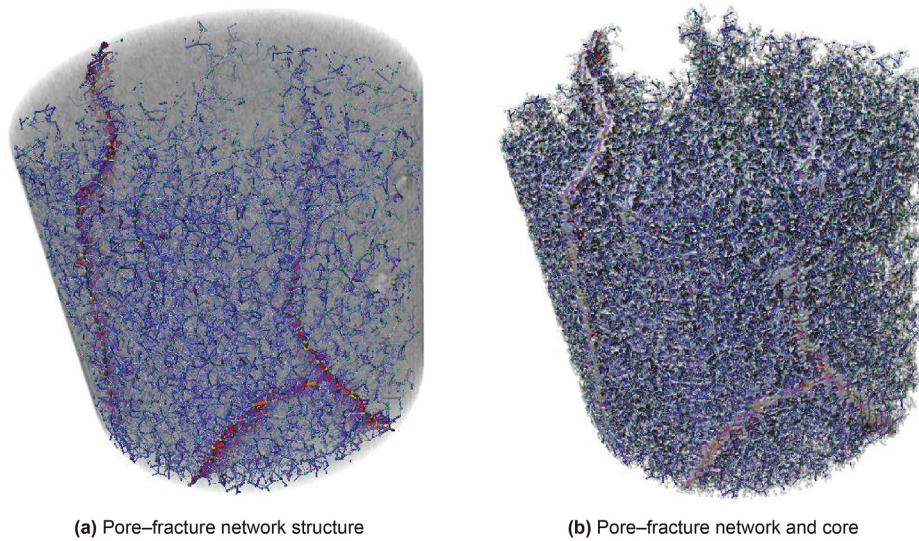


Fig. 10. Pore-fracture network structure.

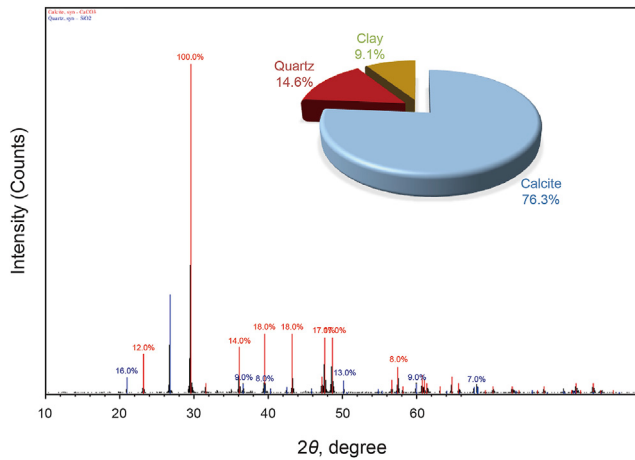


Fig. 11. X-ray diffraction results of the whole rock.

(EDS) test is carried out for the areas with obvious characteristics, as shown in area 1, area 2 and area 3 in Fig. 12. EDS test mainly includes point scanning, line scanning and area scanning. Because the distribution of rock conditions has spatial continuity, this scanning is carried out in the way of area scanning. CT scanning

profile of rock and schematic diagram of EDS scanning area are shown in Fig. 12.

The scanning and EDS results of area 1, area 2, and area 3 are shown in Figs. 13–15.

According to the fixed-point EDS test results and combined with the X-ray diffraction results, it can be analyzed that area 1 is mainly quartz and a small amount of calcite, area 2 is mainly clay minerals, and area 3 is mainly calcite and a small amount of quartz. Using this result, the mineral types in CT map can be classified and corrected manually. Here, the author manually revised five rock profiles and used U-Net model for learning and segmentation. There are few training data here. In the follow-up work, the author will continue to conduct in-depth research in this regard. The distribution of rock conditions is shown in Fig. 16.

The construction of rock mineral distribution is essential for experimental simulation using digital cores. The change in core permeability, damage evaluation, and five sensitivity evaluations are closely related to the distribution of rock minerals in the process of acid displacement. There is no accurate distribution of rock minerals. The development of wormholes is the same in a hydrochloric or soil acid system, but it is not in accordance with the actual situation. Without a more accurate distribution of rock minerals, it is impossible to accurately simulate the expansion of clay minerals, and the corresponding water-sensitive damage cannot be accurately simulated.

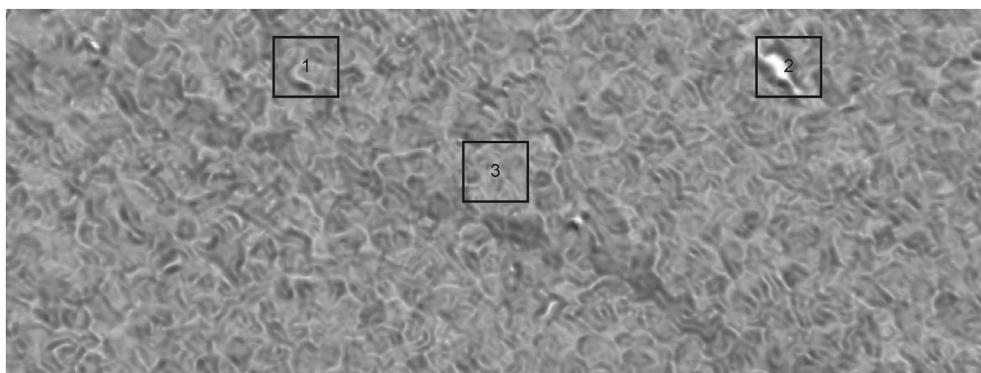


Fig. 12. CT scanning profile of rock and schematic diagram of EDS scanning area.

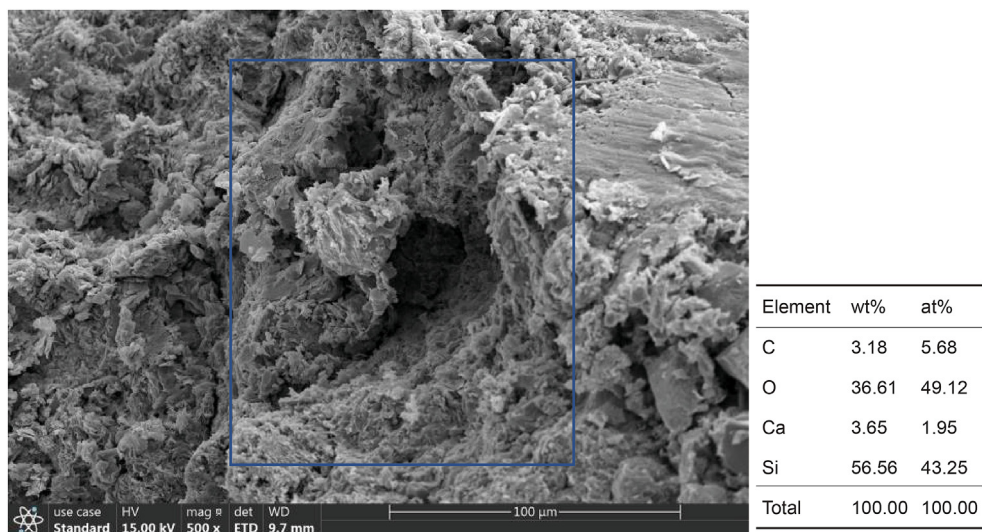


Fig. 13. The scanning and EDS results of area 1.

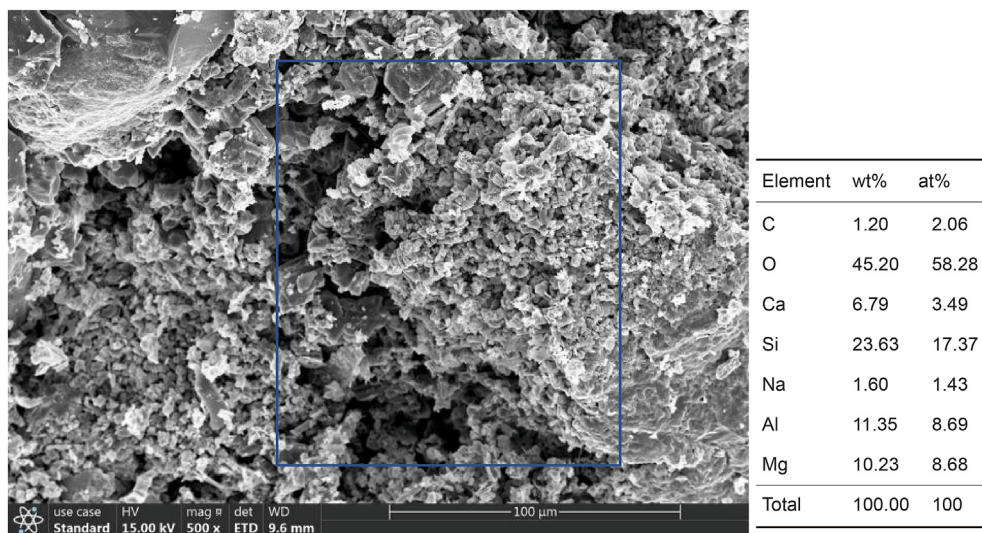


Fig. 14. The scanning and EDS results of area 2.

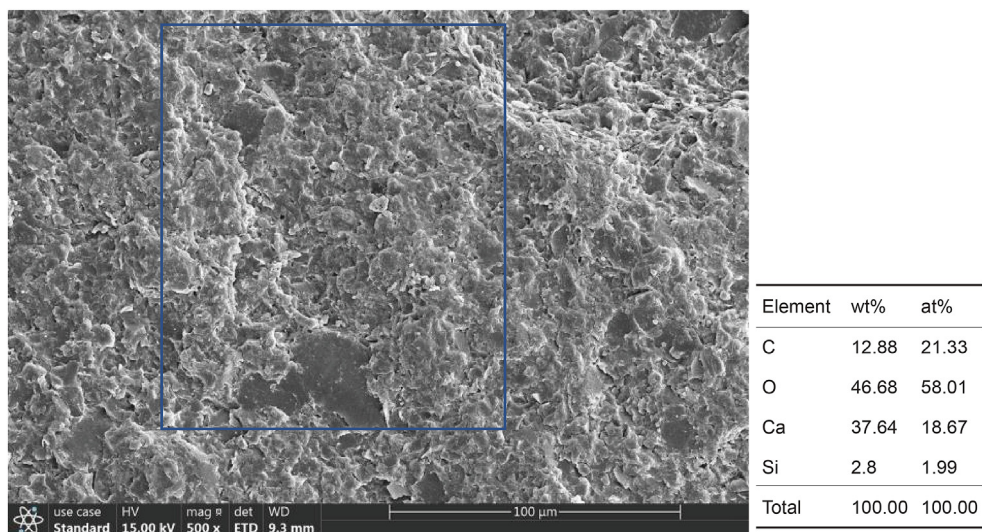


Fig. 15. The scanning and EDS results of area 3.

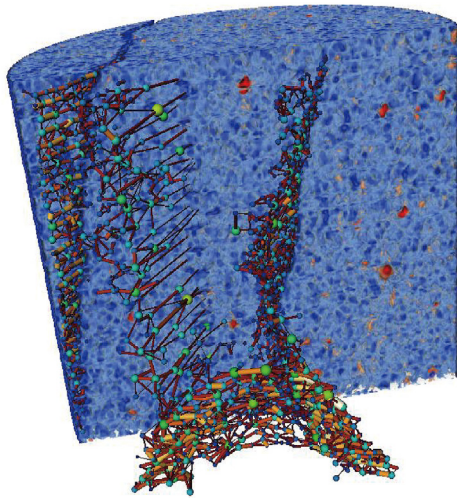


Fig. 16. Distribution of rock minerals of DRP.

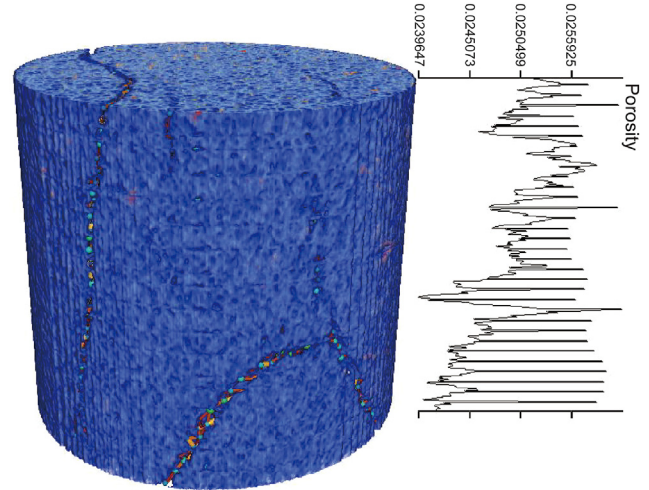


Fig. 18. Vertical distribution of porosity in digital core.

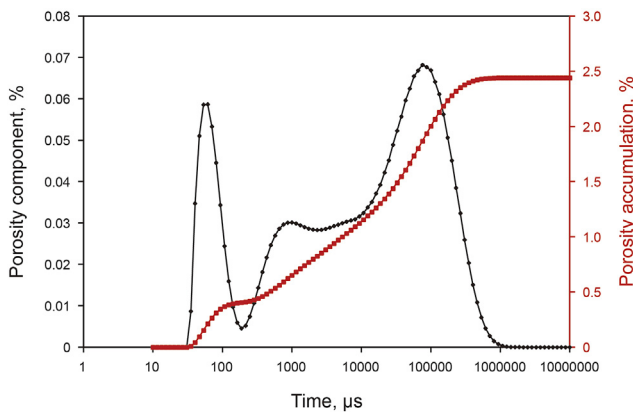


Fig. 17. NMR T_2 spectrum measurement.

8. Model validation

The verification of porosity is the most intuitive and accurate verification parameter. Because the established pore model is based on X-ray CT scanning, with high resolution, and can identify a large number of invalid pores (dead pores), a more accurate porosity measurement method is needed to verify the model. MesoMr23-060H-I NMR instrument was used to measure core porosity. After saturated with water and centrifugation, the NMR T_2 spectrum distribution of the core was measured, as shown in Fig. 17.

The core porosity measured via NMR was 2.44%. The distribution of the T_2 spectrum was mainly bimodal, which indicated that there were mainly small pores and fractures in the core. The left and right peaks represent small pores and fractures, respectively. The contribution rate of pore height mainly came from the fractures.

For the porosity calculation of the digital core, the pore and fracture volumes are used as follows:

$$\phi = \frac{\sum_{i=0}^{n_1} V_{\text{voxelf}_i} + \sum_{i=0}^{n_2} V_{\text{voxelp}_i}}{\sum_{i=0}^{n_1+n_2} V_{\text{voxel}_i}} \times 100\% \quad (9)$$

where ϕ is porosity; V_{voxelf} is the volume of voxels that make up the fracture, μm^3 ; V_{voxelp} is the volume of voxels that make up the

pores, μm^3 ; n_1 is the number of voxels that make up the fracture; n_2 is the number of voxels that make up the pores.

The average porosity calculated via the DRP was 2.57% (Fig. 18), and the relative error was 5.33%. The main reason was that the H core measured via NMR is from the water in the process of core saturated with water, so some dead pores could not be filled with water, which made the porosity measured via NMR smaller than the actual value. Therefore, the relative error of the digital core was less than 5.33%. Thus, the accuracy of the digital core model was very high, and the difference between the digital and actual cores was small.

9. Conclusions

- (1) X-ray CT scanning technology can efficiently reconstruct the 3D structure of the core. For the complex core with fractures, nonlocal means filter technology can reduce noise, retain core detailed characteristics and spatial correlation of physical properties.
- (2) The conventional threshold segmentation technology has a poor recognition effect on the fracture and pore of complex cores, which is one of the critical factors limiting the development of digital cores. The U-Net model has a good semantic segmentation effect, can effectively extract the pore and fracture characteristics of the core, can efficiently segment fractures, pores, and matrix, and can keep the spatial correlation between pores and fractures.
- (3) The modeling of rock mineral distribution mainly uses the U-Net DL model to identify different minerals, which is conducive to the correction of XRD technology. It is indispensable for physical experiment simulation involving acid rock reaction, chemical adsorption, and physical expansion.
- (4) The relative error between porosity measured via NMR and average porosity calculated via DRP was only 5.33%. The main reason was that the H core measured via NMR was water from the process of core saturated with water, so some dead pores could not be filled with water, and the porosity measured via NMR was smaller than the actual value.

Acknowledgments

The authors wish to express their sincere thanks to the Science and Technology Cooperation Project of the CNPC-SWPU Innovation

Alliance (No. 2020CX010501). And National Science and Technology Major Project and National Natural Science Foundation of China Petrochemical Joint Fund Project (U1762107).

References

- Al-Marzouqi, H., 2018. Digital rock physics: using CT scans to compute rock properties. *IEEE Signal Process. Mag.* 35 (2), 121–131. <https://doi.org/10.1109/MSP.2017.2784459>.
- Andr a, H., Combaret, N., Dvorkin, J., et al., 2013. Digital rock physics benchmarks—Part I: imaging and segmentation. *Comput. Geosci.* 50 (1), 25–32. <https://doi.org/10.1016/j.cageo.2012.09.005>.
- Arns, C.H., Knackstedt, M.A., Pinczewski, W.V., Garboczi, E.J., 2002. Computation of linear elastic properties from microtomographic images: methodology and agreement between theory and experiment. *Geophysics* 67 (5), 1396–1405. <https://doi.org/10.1190/1.1512785>.
- Claudio, M., Almqvist, B.S.G., Saenger, E.H., 2012. Digital rock physics: numerical prediction of pressure-dependent ultrasonic velocities using micro-CT imaging. *Geophys. J. Int.* 3, 1475–1482. <https://doi.org/10.1111/j.1365-246X.2012.05437.x>.
- Dvorkin, J., Derzhi, N., Fang, Q., Nur, A., Nur, B., Grader, A., et al., 2009. From micro to reservoir scale: permeability from digital experiments. *Lead. Edge* 28 (12), 1446–1452. <https://doi.org/10.1190/1.3272699>.
- Forkert, N.D., Schmidt-Richberg, A., Fiehler, J., Illies, T., Ehrhardt, J., 2013. 3d cerebrovascular segmentation combining fuzzy vessel enhancement and level-sets with anisotropic energy weights. *Magn. Reson. Imag.* 31 (2), 262–271. <https://doi.org/10.1016/j.mri.2012.07.008>.
- Kalam, Z., Gibrata, M., Hammadi, M.A., Mock, A., Lopez, O., 2013. Validation of digital rock physics based water-oil capillary pressure and saturation exponents in super giant carbonate reservoirs. In: *SPE Middle East Oil and Gas Show and Conference*. Society of Petroleum Engineers. <https://doi.org/10.2118/164413-MS>.
- Karimpouli, S., Faraji, A., Balcewicz, M., Saenger, E.H., 2019. Computing heterogeneous core sample velocity using digital rock physics: a multiscale approach. *Comput. Geosci.* 135, 104378. <https://doi.org/10.1016/j.cageo.2019.104378>.
- Kelly, S., El-Sobky, H., Torres-Verdin, C., Balhoff, M.T., 2016. Assessing the utility of FIB-SEM images for shale digital rock physics. *Adv. Water Resour.* 95 (Sep), 302–316. <https://doi.org/10.1016/j.advwatres.2015.06.010>.
- Knackstedt, M.A., Latham, S., Madadi, M., Sheppard, A., Varslot, T., Arns, C., 2009. Digital rock physics: 3D imaging of core material and correlations to acoustic and flow properties. *Lead. Edge* 28 (1), 28–33. <https://doi.org/10.1190/1.3064143>.
- Kuntz, M., Mareschal, J.C., Lavalley, P., 2000. Numerical estimation of electrical conductivity in saturated porous media with a 2-D lattice gas. *Geophysics* 65 (3), 766–772. <https://doi.org/10.1190/1.1444775>.
- Long, J., Shelhamer, E., Darrell, T., 2015. Fully convolutional networks for semantic segmentation. *IEEE Trans. Pattern Anal. Mach. Intell.* 39 (4), 640–651. <https://doi.org/10.1109/CVPR.2015.7298965>.
- Riepe, L., Suhaimi, M.H., Kumar, M., Knackstedt, M.A., 2011. Application of high resolution micro-CT-imaging and pore network modeling (PNM) for the petrophysical characterization of tight gas reservoirs—A case history from a deep clastic tight gas reservoir in Oman. In: *SPE Middle East Unconventional Gas Conference and Exhibition*. Society of Petroleum Engineers. <https://doi.org/10.2118/142472-MS>.
- Ronneberger, O., Fischer, P., Brox, T., 2015. *U-Net: Convolutional Networks for Biomedical Image Segmentation*. Springer, Cham, doi:10.1007/978-3-662-54345-0_3.
- Saad, N.M., Abu-Bakar, S., Muda, S., Mokji, M., 2011. Automated segmentation of brain lesion based on diffusion-weighted MRI using a split and merge approach. In: *2010 IEEE EMBS Conference on Biomedical Engineering and Sciences (IECBES)*. IEEE. <https://doi.org/10.1109/IECBES.2010.5742284>.
- Saenger, E.H., Enzmann, F., Keehm, Y., Steeb, H., 2011. Digital rock physics: effect of fluid viscosity on effective elastic properties. *J. Appl. Geophys.* 74 (4), 236–241. <https://doi.org/10.1016/j.jappgeo.2011.06.001>.
- Saenger, E.H., Kr ger, O.S., Shapiro, S.A., 2004. Effective elastic properties of randomly fractured soils: 3D numerical experiments. *Geophys. Prospect.* 52 (3), 183–195. <https://doi.org/10.1111/j.1365-2478.2004.00407.x>.
- Saxena, N., Hows, A., Hofmann, R., Alpak, F.O., Freeman, J., Hunter, S., et al., 2018. Imaging & computational considerations for image computed permeability: operating envelope of digital rock physics. *Adv. Water Resour.* 116 (JUN), 127–144. <https://doi.org/10.1016/j.advwatres.2018.04.001>.
- Schembre, J.M., Kovscek, A.R., 2003. A technique for measuring two-phase relative permeability in porous media via X-ray CT measurements. *J. Petrol. Sci. Eng.* 39 (1), 159–174. [https://doi.org/10.1016/S0920-4105\(03\)00046-9](https://doi.org/10.1016/S0920-4105(03)00046-9).
- Shirangi, M.G., Durlafsky, L.J., 2015. Closed-loop field development under uncertainty by use of optimization with sample validation. *SPE J.* 20, 908–922. <https://doi.org/10.2118/173219-PA>, 05.
- Stadlbauer, A., Moser, E., Gruber, S., et al., 2004. Improved delineation of brain tumors: an automated method for segmentation based on pathologic changes of ¹H-MRSI metabolites in gliomas. *Neuroimage* 23 (2), 454–461. <https://doi.org/10.1016/j.neuroimage.2004.06.022>.
- Taud, H., Martinez-Angeles, R., Parrot, J.F., Hernandez-Escobedo, L., 2005. Porosity estimation method by X-ray computed tomography. *J. Petrol. Sci. Eng.* 47 (3–4), 209–217. <https://doi.org/10.1016/j.petrol.2005.03.009>.
- Zhao, S., Zhou, M., Jia, T., Xu, P., Wu, Z., Yun, T., et al., 2014. Multi-branched cerebrovascular segmentation based on phase-field and likelihood model. *Comput. Graph.* 38, 239–247. <https://doi.org/10.1016/j.cag.2013.11.004>. Feb.